Mechanochemical Synthesis Of Anatase-Rutile Phases At Ball Milling In Different Conditions And Its Cause And Effect On A Photo-Oxidation Process

Síntese mecanoquímica das fases anatase-rutilo em um moinho de bolas em diferentes condições e suas causas e efeitos em um processo de foto-oxidação

DOI:10.34117/bjdv7n1-142

Recebimento dos originais: 05/12/2020
Aceitação para publicação: 08/01/2021

Jean César Marinozi Vicentini
Dr. in Chemical Engineering
State University of Maringa
Chemical Engineering Department, State University of Maringa, Colombo Avenue, 5790, 87020-090, Maringa, Parana, Brazil
E-mail: jcmarinozi@gmail.com

Gimerson Weigert Subtil
Ms. in Chemical Engineering
State University of Maringa
Chemical Engineering Department, State University of Maringa, Colombo Avenue, 5790, 87020-090, Maringa, Parana, Brazil
E-mail: weigert_subtil@hotmail.com

Daiane Marques de Oliveira
Ms. in Chemical Engineering
State University of Maringa
Chemical Engineering Department, State University of Maringa, Colombo Avenue, 5790, 87020-090, Maringa, Parana, Brazil
E-mail: daiane.marques20@gmail.com

Fernanda de OliveiraTavares
Dr. in Chemical Engineering
State University of Maringa
Chemical Engineering Department, State University of Maringa, Colombo Avenue, 5790, 87020-090, Maringa, Parana, Brazil
E-mail: fernandatavares15@gmail.com

Mara Heloisa Neves Olsen Scaliante
Dr. in Sciences
State University of Maringa
Chemical Engineering Department, State University of Maringa, Colombo Avenue, 5790, 87020-090, Maringa, Parana, Brazil
E-mail: mhnoscaliante2@uem.br

Marcos de Souza
Dr. in Chemical Engineering
State University of Maringa
Chemical Engineering Department, State University of Maringa, Colombo Avenue, 5790, 87020-090, Maringa, Parana, Brazil
E-mail: msouza2@uem.br

ABSTRACT
This study aims to evaluate the effect of the grinding parameters applied to TiO2 comminution, which forms a heterojunction of anatase-rutile phases and reduces markedly the size particle. This material is a well-knowm photocatalyst in environmental issues such as degradation of synthetic dyes, mainly due to the large surface area and oxidative radicals generations ability. The influence of time, rotational speed and the solvent was investigated in the grinding process. Catalysts were prepared by a deposition method and were characterized by XRD, textural analysis (BET area), potential electrophoretic, photoacoustic and Mössbauer spectroscopy. The comminution procedure reduced the size of TiO2 crystallites from 87 nm to 22 nm as well as the surface area and pore diameter. The best photocatalytic activity was for TiO2 comminuted for 10 min and 300 rpm in a dry medium supported on ZSM-5. It was registered that the photoactivity of TiO2 decreased with the transition of anatase to rutile phase and also by the iron oxides insertion during the comminution process. This study has a great technologic contribution because it elucidates primary issues on the particle sizes reduction in the catalysts production, whose function is to have a better metal distribution on the support's surface.

Keywords: ZSM-5, photocatalysis, pseudobrokita, Mössbauer Spectroscopy, grinding.

RESUMO
Este estudo visa avaliar o efeito dos parâmetros de moagem aplicados à cominuição do TiO2, que forma uma heterojunção de fases anatase-rutilo e reduz acentuadamente o tamanho da partícula. Este material é um fotocatalisador bem conhecido em questões ambientais como a degradação de corantes sintéticos, principalmente devido à grande área de superfície e à capacidade de geração de radicais oxidantes. A influência do tempo, da velocidade de rotação e do solvente foi investigada no processo de moagem. Os catalisadores foram preparados por um método de deposição e foram caracterizados por DRX, análise textural (área BET), potencial eletroforético, fotoacústico e espectroscopia Mössbauer. O procedimento de cominuição reduziu o tamanho dos cristais de TiO2 de 87 nm para 22 nm, assim como a área de superfície e o diâmetro dos poros. A melhor atividade fotocatalítica foi para TiO2 cominuído durante 10 min e 300 rpm em meio seco suportado em ZSM-5. Foi registrado que a fotoatividade do TiO2 diminuiu com a transição da fase anatase para a fase rutilo e também pela inserção de óxidos de ferro durante o processo de cominuição. Este estudo tem uma grande contribuição tecnológica porque elucida questões primárias sobre a redução do tamanho das partículas na produção de catalisadores, cuja função é ter uma melhor distribuição do metal na superfície do suporte.

Palavras-chave: ZSM-5, fotocatálise, pseudobrokita, Espectroscopia Mössbauer, moagem.

1 INTRODUCTION

Population growth, urbanization, industrialization and men's persistence to search for a life with more comfort, benefits and achievements associated with the vulnerability of social, economic and environmental systems have caused a growing environmental imbalance. The industrial process in textile industry is known for consuming huge amounts of water, fuels, dyes and other chemicals to achieve the commercial standard fibers. The discharge of water effluents, containing dyes, into water ecosystems, creates an ecological imbalance, even in small concentrations, affecting the aesthetic and water quality standards. The dyes contain a high COD and BOD load, which gives these compounds one characteristic: to be recalcitrant for single water conventional treatments. Brites & Nobrega reported that a concentration of only 5 μg/L of reactive dye can block solar radiation in the bed of water bodies, and thus decrease the concentration of O_2 dissolved, resulting in the eutrophication of this receptor body [1]. According to Körlü and co-authors, in an industrial laundry of denim located in Söke (Turquey) in 2015 presented an effluent with a COD charge of 1300 mg/L[2].

An effective alternative to treat wastewater can be found with an Advanced Oxidation Process (AOP). Heterogeneous photocatalysis is an AOP technique which consists of activating a semiconductor with light radiation to promote the e^-/h^+ pairs formation and further the generation of transient species through water hydrolysis. These transient species, named as radicals, are very efficient in the mineralization of a wide range of recalcitrant organic compounds. Vicentini and collaborators achieved a photodiscoloration greater than 95% of an artificial solution of reactive blue dye (10 ppm) in less than 5 h of light exposure applying TiO2 immobilized on NaA as photocatalyst, while the amount adsorbed by the same material was considered negligible, thus confirming the superiority of AOP against adsorption in the removal of dyes [3]. Znad and co-authors achieved complete discoloration of a 20 ppm orange methyl solution in 180 min and a 99% reduction in total organic carbon in a solar simulator using TiO_2 immobilized in ZSM-5 [4]. Subtil and co-authors also achieved complete dye mineralization in a few minutes of radiation using nano-TiO_2 immobilzed in ZSM-5 [5]

The TiO_2 was established as the most used catalyst owing to its set of features like photostability, corrosion resistance and low cost. Znad, for example, proved the strong stability of the TiO_2-based catalyst in up to 6 reaction cycles, maintaining the removal of methyl orange above 95%. [4]. Saggioro and coauthors observed that there was a reduction from 98% to 80%, in the removal of the indigo-carmine dye, in 5 reaction cycles

using TiO_2 as catalyst [6]. There are several ways of enhancing the photocatalytic yield of the pollutants degradation; the reaction conditions can be altered: radiation time, light source, auxiliary oxidizing agents, O_2 bubbling insertion, solution pH adjustment, reaction temperature, reactor shape and catalyst concentration. Besides that, the catalyst can be improved by reducing the size of its particle to promote greater surface area and immobilizing metals and non-metals to increase the light absorption spectrum and delay the main deactivating effect of the catalysts, the electronic recombination.

The size reduction of catalysts is an interesting way to improve the titanium performance, causing a better surface distribution of the catalyst and establishing more active sites. Goedecke and collaborators concluded in their research that the particle size of TiO_2 directly influences the efficiency of the photocatalytic process. It was observed that there was a complete discoloration of a methylene blue solution applying particles in a range of 20 nm ≤ dp ≤ 50 nm, compared to only 60% of dye removal (approximately) when use the bigger ones (200 nm ≤ dp ≤ 400 nm) [7]. In the grinding process, for example, products can be influenced by several factors that imply grain size and formation of new compounds, such as the type of mill, the composition of the bowl and the grinding balls, the rotation speed, the grinding time, the mass ratio between grinding balls and processed sample, the grinding atmosphere, process controlling agents , the filled volume of the grinding vessel and the temperature of the grinding medium. [8]. The milling procedure consists of a mechanism of cold welding, in which the crystallites are broken and welded simultaneously without changing their physical state. The reduction of crystallites happens when the ‘fracture mechanism’ is greater than the ‘welding mechanism’, while the agglomeration happens with the opposite procedure, increasing the crystallite size [8].

Anand et al. (2015) studied the reduction of ZnO particle size over wet milling using Dispersol F as a wet medium in 3 different concentrations, 2%, 3% and 4% (g of Dispersol F/g of distilled water). The authors found that independent from the concentration of the surfactant the reduction in the particle size is observed up to a time equivalent to 6 h of grinding, after that the particles begin to aggregate and increase a little in size. This could be explained by the cold welding mechanism having detached itself from the fracture mechanism. The greater dispersion caused by the higher concentration of Dispersol F makes the agglomeration of particles difficult [9]. The same was identified by Jung et al (2015) in the comminution of boron particles in a mixer mill. Starting from particles approximately 800nm in size, in the dry grind after 4 h they

reached an average of 58 nm, while in the wet one, with hexane and oleic acid, 220nm. The authors justified that when in wet grinding, due to the viscosity of the agent, there is damping of the impact of the balls between the particles, decreasing the speed of their reduction [10].

One disadvantage of reducing the particles size by a grinding process is the contamination of the processed material by the grinding jar and balls composition. Furlani and coauthors (2014) in a part of his study evaluated the grinding of titania (Aldrich) in a SPEX mill using a zirconia grinding vessel and alumina balls, and at the end of the processing reported the presence of metals from the grinding medium in the processed material [11]. Dabhade and collaborators (2007) identified in the final titania samples treated for 75 h in an Attritor type mill the presence of the following metal in the processed material: Fe = 1.15%, Cr = 0.26%, Ni = 0.18%, Mn = 0.11%. They also reported that the contamination is proportional to the milling time [12].

When a metal oxide is milled, a mechanochemical synthesis (caused by different temperature points inside the grinding vessel) can occur and may establish phase changes formations and, therefore, modify the physicochemical, optical and electronic properties of the processed material. There are two types of temperatures in a grinding mechanism process, the macroscopic temperature that assumes an absolute temperature value around 40 °C, and the microscopic temperature which can reach temperatures above 1000 °C [8]. Miszczak e Pietrzyk [13] and Rodríguez-Torres *et al* [14] observed that when TiO_2 was comminuted (fully in the anatase phase), under various milling parameters, in addition to the reduction in particle size, the transformation of that to the rutile phase occurred. This transformation is explained according to the authors by the microscopic temperature, since the phase change temperature (in a muffle furnace) identified for titanium in the literature is in the range of 700 °C [15].

Kordouli and researchers reported that a mixture of TiO_2 anatase and rutile phases, synthetized with different calcination temperatures, form a heterojunction between the phases and the Anatase/Rutile ratio equal to 0.8 had the best results on the photocatalytic activity of dye solution, caused by the improvement of electronic transfer from anatase to rutile and the adsorptive properties [16]. Besides that, in the photocatalysis, the smallest particle size can imply better metal oxide distribution along the support surface in comparison with the largest one, and thus ensure more physical strength to improve the photocatalytic activity. In virtue of their small size, titanium dioxide particles are difficult to remove from the medium after a reaction is completed. Centrifugation or filtration are

efficient procedures to remove these particles; however, they can entail considerable expenses. The catalyst immobilization on supports generally facilitates the separation and enables the reutilization [17].

The zeolite ZSM-5 type is one of the most commonly used inorganic materials as a catalyst support, molecular sieve and adsorbent. The ZSM-5 is characterized by being ecologically clean, inert, non-toxic and by having high porosity, strong proton acidity and the capacity of exchanging compensating cations [18]. The ZSM-5 acidity is defined by the Si/Al ratio of the zeolitic structure.

The objective of this paper was to evaluate the TiO_2 particles size reduction by combining the grinding parameters: time, rotational velocity and grinding media. It was also to discuss the positive and negative effects of the other changes that occur in a mechanochemical process of grinding through characterization and the material processed application in a photo-oxidative process.

2 MATERIAL AND METHODOS

2.1 MATERIALS

The chemicals used were titanium dioxide (Kronos, 100% Anatase); sodium hydroxide (reagent grade, ≥97%, Vetec); silica (AEROSIL 380); zeolite ZSM-5 seed (SR98 - courtesy CENPES, Petrobrás); aluminum sulfate $Al_2(SO_4)_318H_2O$ (reagent grade, ≥97%, Synth); ethil alcohol (reagent grade, ≥99.5%, Synth); reactive blue dye (RB250); acetone (reagent grade, ≥99.5%, Synth).

2.2 TIO_2 COMMINUTION IN PLANETARY BALL-MILLING

The titanium dioxide was treated in a Pulverisette Planetary ball-milling 6 (Fritsch) using a fixed ratio of 30:1 (g/g) between mass balls and mass of titanium dioxide. The varied parameters were: grinding time (10 min, 30 min, 2 h and 6 h), rotational speed (300 rpm and 400 rpm) and the grinding medium (dry or with acetone). An extend investigation about the grinding parameters was done as an initial study (Table 2). The results from initial study were used to choose the parameters for the photocatalytic test. The grinding jar has a volume of 80 mL and made of a 0.70Fe-0.18Cr-0.09Ni alloy steel and the balls made of chrome steel (D.15 mm).

2.3 ZSM-5 SYNTHESIS

The synthesis of ZSM-5 zeolite with Si/Al ratio equal to 30 was performed by a gel synthesis method. It was used 178.65 g of deionized water, 1.5 g seeds of ZSM-5, 15 g SiO_2, 2.83 g of aluminum sulfate, 3.6 g of sodium hydroxide and 11.5 g of ethyl alcohol. First, the ZSM-5 seeds were dispersed in deionized water and immediately the solution was equally separated into two beckers, (i) and (ii). It was added silica into becker (i) and aluminum sulfate into becker (ii). After homogenization, the solutions from both beckers were mixed into just one. Then, ethyl alcohol and sodium hydroxide were added into this solution. The mixture was homogenized for 20 min and then inserted in an autoclave at temperature of 170 °C for 4 days, then filtered, washed several times with deionized water, dried at 100 °C and calcined at 500 °C for 5 h.

2.4 CATALYST PREPARATION

The catalysts were prepared by physical deposition method. The zeolite and TiO_2 samples, previously dried at 100 °C for 1 day, were placed in a volumetric flask with deionized water. Then they were dried completely in a rotary evaporator at 70 °C under vacuum and then left in an oven at 100 °C for 12 h. The catalysts were calcined at 500 °C for 5 h. The final product had 0.07 g/g (7%) of TiO_2 supported on ZSM-5.

The prepared catalysts nomenclature was presented at Table 1.

Table 1. Supported and non-supported catalysts symbols.

Prepared catalysts	
TiO_2 Kronos (wm)[a]	ZSM-5/(TiO_2)
TiO_2 (10 min/300 rpm/dry)[b]	ZSM-5/(TiO_2) (10 min/300 rpm/dry)
TiO_2 (30 min/300 rpm/dry)	ZSM-5/(TiO_2) (30 min/300 rpm/dry)
TiO_2 (2 h/300 rpm/dry)	ZSM-5/(TiO_2) (2 h/300 rpm/dry)
TiO_2 (6 h/300 rpm/dry)	ZSM-5/(TiO_2) (6 h/300 rpm/dry)
TiO_2 (6 h/400 rpm/dry)	ZSM-5/(TiO_2) (6 h/400 rpm/dry)
TiO_2 (6 h/400 rpm/wet[c])	ZSM-5/(TiO_2) (6 h/400 rpm/wet)

[a]wm (without milling); [b]grinding parameters (time, speed, medium); [c]wet (milling with acetone).

2.5 CATALYST CHARACTERIZATION

The X-ray diffractions (XRD) were obtained using an X-ray diffractometer Bruker D8 Advance 2θ from 5° to 85°, CuKα radiation, 0.24 °/min, 40 kV and 50 mA with the aid of the database ICDD PDF2 (Philips) Software Xpert Score. Textural properties were determined by physical adsorption isotherms of N_2 using the Quantachrome apparatus.

The sizes of the different TiO_2 crystallites were also determined by XRD from Scherrer Equation [19] and particles size of TiO_2 by Dynamic Light Scattering (DLS) using an ALV/CGS-3 compact goniometer. The band gap energy of the catalysts was obtained by photoacoustic spectroscopy. The concentrations of iron ions (major component of vessel grinding composition) were measured by atomic absorption spectrometry in flame on Spectra AA, 50B model Varian. The zeta potential was determined by electrophoretic light scattering (ELS) using the Zetasizer NanoZS apparatus. Mössbauer spectroscopy was applied to determine the type of iron contamination on TiO_2 after grinding process.

The proton acidity was measured by desorption of NH_3 under temperature programmed (DTP-NH_3) in CHEMBET 3000 Quantachrome Apparatus. Briefly, 100 mg of each sample was subjected to a pre-treatment at a temperature of 300 °C, with nitrogen flow, at a flow rate of 20 mL/min, for 1 h, to remove the adsorbed water. Then, the ammonia adsorption was carried out at 100 °C for 30 min. Then, the physiosorbed ammonia was removed with constant N_2 flow for 2 h. The desorption of chemosorbed NH_3 was monitored at a rate of 10 °C/min and the final temperature was 700 °C. The signal obtained were plotted against time and by the integral of the curve was calculated the total acidity of each sample in mmol $NH_3/g_{catalyst}$.

2.6 PHOTOCATALYTIC TESTS

The photocatalytic tests were performed in according to Vicentini et al. [3].Briefly, the tests were carried out in a glass reactor filled with 250 ml of dye solution (10 mg/L) containing 1 g/L of supported catalysts. The reactional medium was irradiated with a mercury vapor lamp (250 W) for a preferable UV radiation emission. The temperature of the reaction was maintained at approximately 25 °C with a cooling system. Aliquots were taken at regular time intervals of 1 h for a 5h total period of irradiation time, filtered with Millipore 0,22 μm membranes and analyzed using UV-Vis spectrophotometry (DR 2700 - HACH). The tests were done in duplicate. Percentage of discoloration was calculated by the Equation 1. The dye absorbance was determined at 617 nm wavelength.

$$Decolorization(\%) = \frac{C_i - C}{C_i} \quad (1)$$

Where Ci is the initial concentration of dye at t = 0 and C is the concentration during the irradiation intervals. In order to observe which reaction order best fits the data, first and second order kinetics were proposed. The 1st order kinetics of the reaction was determined by Equation 2 [1,3].

$$Ln\ \frac{C_i}{C} = kt \tag{2}$$

The 2nd order kinetics (Equation 3) of the reaction was also calculated to evidence the character of order reactions from dyes solution discoloration.

$$\frac{1}{C} = kt + \frac{1}{C_i} \tag{3}$$

3 RESULTS AND DISCUSSION

From Table 2, it was possible to identify that the phase transformation of anatase to rutile and the reduction of the TiO_2 crystallite diameter only happened at a dry medium condition.

Table 2. An extend study of the grinding parameters on TiO2 comminution. Percentage of Anatase-Rutile phases and its respective crystallite diameters determined by Scherrer's equation [19].

Samples	%TiO_2		$D_{CRYSTALLITE}$ (nm)	
	Anatase	Rutile	Anatase	Rutile
TiO_2 Kronos (wm[a])	100	0	87	--
10min/300rpm/dry[b]	100	0	59	--
30min/300rpm/dry	100	0	34	--
1h/300rpm/dry	98.9	1.1	25	80
2h/300rpm/dry	83.4	16.6	22	9.0
6h/300rpm/dry	20.2	79.8	19	8.2
10min/400rpm/dry	100	0	47	--
30min/400rpm/dry	91.5	8.5	24	14
1h/400rpm/dry	42.1	57.9	21	8.1
2h/400rpm/dry	13.9	86.1	19	8.4
6h/400rpm/dry	0	100	--	8.8
10min/300rpm/wet	100	0	86	--
30min/300rpm/wet	99	1	84	8.5
1h/300rpm/wet	100	0	84	--
2h/300rpm/wet	100	0	84	--
6h/300rpm/wet	100	0	82	--
10min/400rpm/wet	100	0	85	--
30min/400rpm/wet	100	0	84	--
1h/400rpm/wet	100	0	84	--
2h/400rpm/wet	100	0	84	--
6h/400rpm/wet	100	0	83	--

[a]wm: without milling, [b]grindind parameters (time, speed and grinding medium).

Then, from Table 2 were chosen the conditions that occur the titanium phase transformation and the crystallite size reduction, for later synthesize their respective supported catalysts (from right column of Table 1).Figure 1 shows the XRD of TiO_2 samples (catalysts from the left column of Table 1). It follows that there is a reduction in crystallinity compared to the non-treated sample by the diminution of the peak intensity and also a broadening of the peaks indicated more amorphous materials. At XRD (Figure 1), TiO_2 anatase phase peaks were observed, such as at $2\theta = 25°$, 38°, 48°, 54°, 55°, 63°, and rutile phase peaks at $2\theta = 27°$, 36°, 41°, 54.5° [4,11,20–25].

Figure 1. XRD for unsupported catalysts

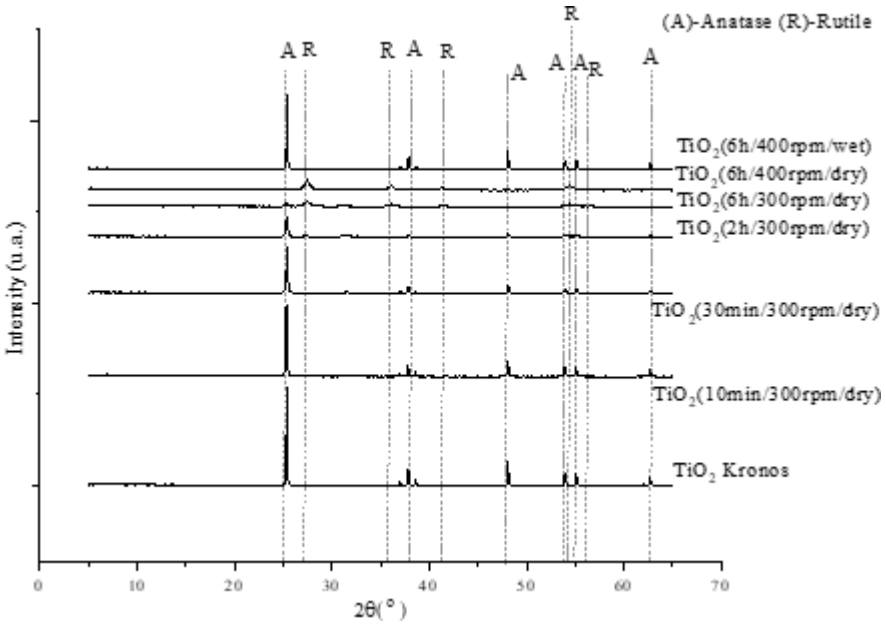

A phase transformation from anatase to rutile was observed. All these observations can be more visible as the energy of the grinding treatment increases. In the wet milling, the acetone acts as process controlling agent (PCA), controlling the temperature, as a result none, or very little, phase change occurs, as can be observed on Table 2 and Table 3.

Table 3. TiO2 composition, band gap energy, grain diameter and iron concentration for TiO2 samples treated in the milling.

Ref.	%Anatase	%Rutile	Band gap (eV)	$D_{cryst.}$ (Anatase)	$D_{cryst.}$ (Rutile)	%Fe
TiO_2 Kronos	100.0 %	0.0 %	3.2	87nm	--	0.000
10 min/300 rpm/dry[a]	100.0 %	0.0 %	3.2	58 nm	--	0.021
30 min/300 rpm/dry	98.2 %	1.8 %	3.2	31 nm	22 nm	0.022
2 h/300 rpm/dry	76.2 %	23.8 %	3.2	22 nm	8 nm	0.064
6 h/300 rpm/dry	11.2 %	88.8 %	3.1	26 nm	8 nm	0.101
6 h/400 rpm/dry	0.6 %	99.4 %	3.1	81 nm	9 nm	0.540
6 h/400 rpm/wet	98.1 %	1.9 %	3.0	81 nm	9 nm	0.700

[a] TiO2 samples treated at ball-milling with those conditions.

The presence of iron in the treated samples is due to material friction from the vessel and the grinding balls (Table 3). The greater the energy of the grinding process, the greater the attrition and the iron species insertion in the material. Iron oxides were identified in low concentrations on Figure 1 (e.g. between the values of $2\theta = 31^{o}$ and 35^{o}). Iron quantification was obtained by atomic absorption and the data was allocated also in Table 3. Although the sample treated with acetone involves less energy than those grinded under dry conditions, there was a high iron contamination from this sample. Acetone surrounding the particles decreases the possibility of comminution but not the iron insertion into the TiO_2 lattice.

The average crystallite diameter, on Table 3, was determined by Scherrer's equation [19]. As the phase transformation occurred, there was a further reduction of the particle size by increasing milling time and rotational speed. The reduction size reached 75%, from 87 nm to 22 nm.

Grinding time greater than or equal to 6 h with equal or higher speed than 300 rpm leads to the dominance of the welding mechanism or agglomeration process. The TiO_2 sample grinded at a wet medium with acetone had little significant reduction because the treatment was performed on wet milling, which dampens the collision within the grinding vessel due to viscosity of the fluid, as discussed by Jung *et al* [10].

When calculating the band gap energy of the catalysts using Tauc's equation [26] it was found that for the TiO_2 samples there was a redshift from 3.2 to 3.0 eV, caused by the phase change of anatase to rutile and also by the presence of iron oxides [15]. The separation of this effects on band gap energy value were not possible. It was possible to verify on Table 3 that the best way to describe the TiO_2 particle size is with the percentage

of iron oxides present in the sample. The higher the iron concentration, the greater the magnetic interaction between the particles, which results in large particle sizes.

In order to observe the size heterogeneity of the TiO_2 grinded samples, or the index of particles polydispersion, DLS measurements was evaluated and its results were displaced in Figure 2. The DLS technique is effective for detecting temporal fluctuations in the scattered light intensity due to fluctuations in concentration and density of sample. This observation is justified by the particles movements in TiO_2 solution suspension, so their scattering light were directly related to the Brownian movement, where smaller particles move faster than larger particles [27].The dispersion confirms that the grinding process does not ensure the same particles size distribution from all the samples, like indicated from the area below the curves. All of the samples increased the hydrodynamic radius mean, in comparison of TiO_2 Kronos. This is justified because the iron oxides insertion, that implies in more electrostatic interaction with water, pushing the hydrodynamic radius mean values up.

Figure 2. Hydrodinamic radius or Stokes radius from TiO2 particles.

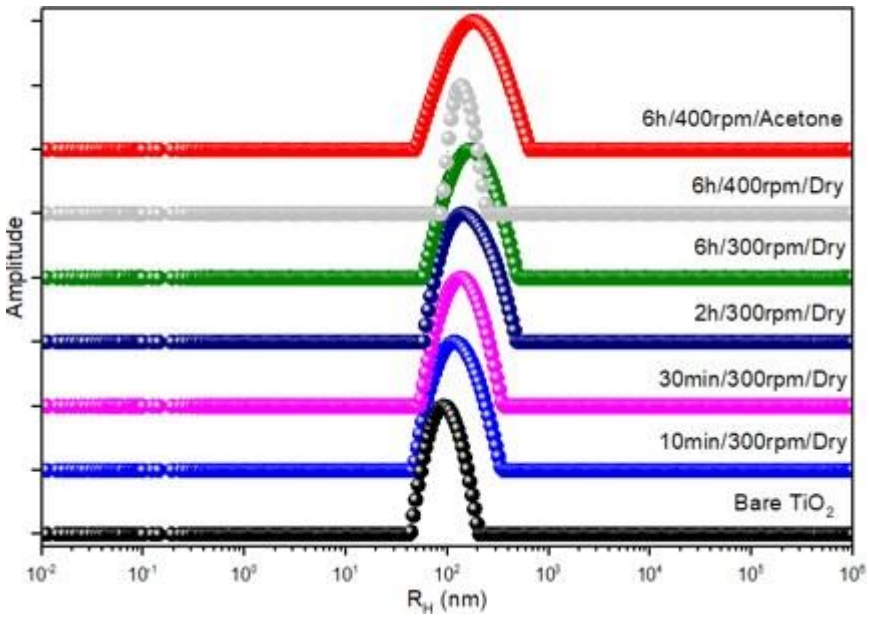

In the X-ray diffraction analysis of the supported catalysts (right column of Table 1), it was possible to observe a slight reduction in the intensity of the XRD peaks when compared to the pure ZSM-5 sample (Figure 3), but no zeolite structure rupture were identified [4]. This reduction in intensity was due to the deposition of the TiO_2 samples on the supports surface. The peaks relating to the active phase of the catalyst (TiO_2

samples) are difficult to identify because of low concentrations of metal oxide used (7 %), but the main peaky were marked in Figure 3, like discussed in Figure 1 [20].

Figure 3. XRD for ZSM-5 and supported catalysts

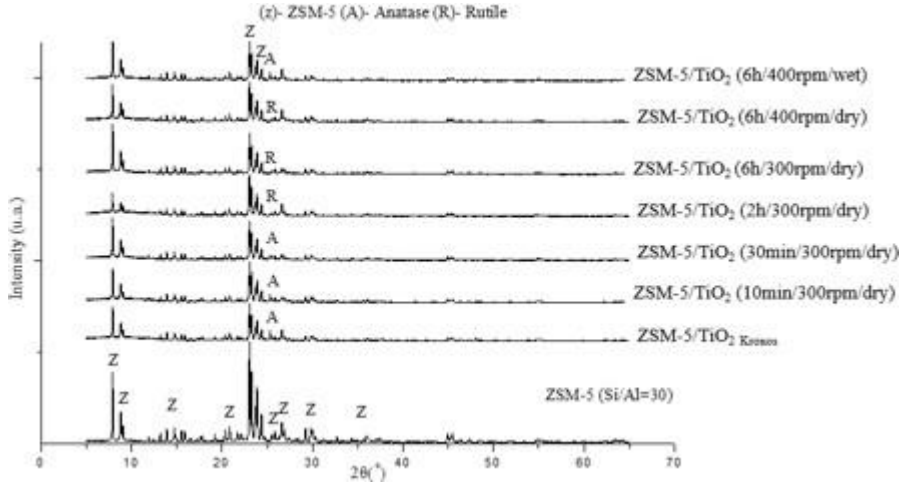

A textural analysis indicated a diminution of the total BET area, also a reduction on the micropore surface area, on the micropore volume and on the average pore diameter after the physical deposition of TiO_2 on the support, compared with pure zeolite, caused by surface recovering (Table 4) [3,25,28].

Table 4. Textural analysis, band gap energy, titanium concentration and Si/Al ratio for pure zeolite and supported catalysts.

Ref	S_{BET}[a] (m^2/g)	S_{micr}[b] (m^2/g)	V_{micr}[c] (cm^3/g)	D_p[d] (Å)	Band gap (eV)	mmol NH_3/gcat
ZSM-5(30)	328	287	0.13	5.7	4.5	1.1215
TiO_2/ZSM-5(30)	263	217	0.12	6.9	3.3	0.9055
10 min/300 rpm/dry[e]	271	249	0.12	4.7	3.3	0.9557
30 min/300 rpm/dry	351	308	0.15	5.9	3.3	0.9539
2 h/300 rpm/dry	244	208	0.09	5.3	3.2	0.9487
6 h/300 rpm/dry	302	279	0.12	4.2	3.1	0,9205
6 h/400 rpm/dry	274	239	0.10	5.4	3.0	0.8922
6 h/400 rpm/wet	385	304	0.14	7.9	3.2	0.9181

[a] Total BET surface area ($0,1 \leq P/P0 \leq 0,3$), [b] micropore surface area, [c] micropore volume, [d] pore diameter, [e] TiO2 milled with those conditions and supported at 7% w/w on ZSM-5.

An increase of the total BET area was identified in just two catalysts (10min/30rpm/dry and 6h/400rpm/wet), owing to the loss of amorphous material during the calcination steps of metal-oxide deposition on ZSM-5. The band gap energy on Table 4 for zeolite ZSM-5 does not necessarily indicate the value of the excitation energy of the valence band electrons. Zeolites are not semiconductors, so the calculated energy is

related to excitation of aluminum atoms in the zeolite structure [29]. The reduction of the band gap energy along with the deposition of TiO_2 is due to the synergic effect between the zeolite and the titanium. The deposition of the catalyst can produce nanocrystals in the channels and pores of the zeolite resulting in lower energy absorption of photons as observed by the reduction in the micropore volume after deposition [3] (Table 2).

The proton acidity by ammonium chemisorption was prepared for those supported catalysts (from right column of Table 1) to verify the behavior of the TiO_2 physical deposition on ZSM-5. The reduction in acidity is explained by the occupation of zeolite acid sites by the TiO_2 samples (Table 4).

The measurement of zeta potential was determined by electrophoresis for pristine ZSM-5, non-treated TiO_2, treated TiO_2, and for supported catalysts (the pH of deionized water used was 6). All of them are shown on Figure 4. It was found that the isoelectric point for pristine TiO_2 was at pH equal to 6.3, within the range of 6 - 6.8, as reported by Kosmulski [30]. For the TiO_2 sample treated at 6h/400rpm/wet, the isoelectric point was at a pH of 4.5. This reduction in the value of the isoelectric point between the TiO_2 samples, treated and non-treated, can be explained by the reduction of the particles size and the iron oxides contamination. Pristine zeolite has the isoelectric point at pH equal to 4.0, very close to that reported by Kosmulski [31]. After the TiO_2 deposition, the pH decreases to 2.0 for both catalysts ZSM-5/TiO_2 and ZSM-5/TiO_2 (6h/400rpm/wet). Since the pH of RB250 dye solution is equal to 6.0, both supported and non-supported catalysts present negative surface charge, which impedes the adsorption of dyes on the surface, caused by the electrostatic repulsion exerted by the negative charge of sulphonic groups present in the dye structure (Figure 4A) [4].

Figure 4. Zeta potential for (a) zeolite, supported and non-supported catalysts and (b) supported and non-supported catalyst (6h/400rpm/wet). The Reactive blue dye structure is also showed in (a).

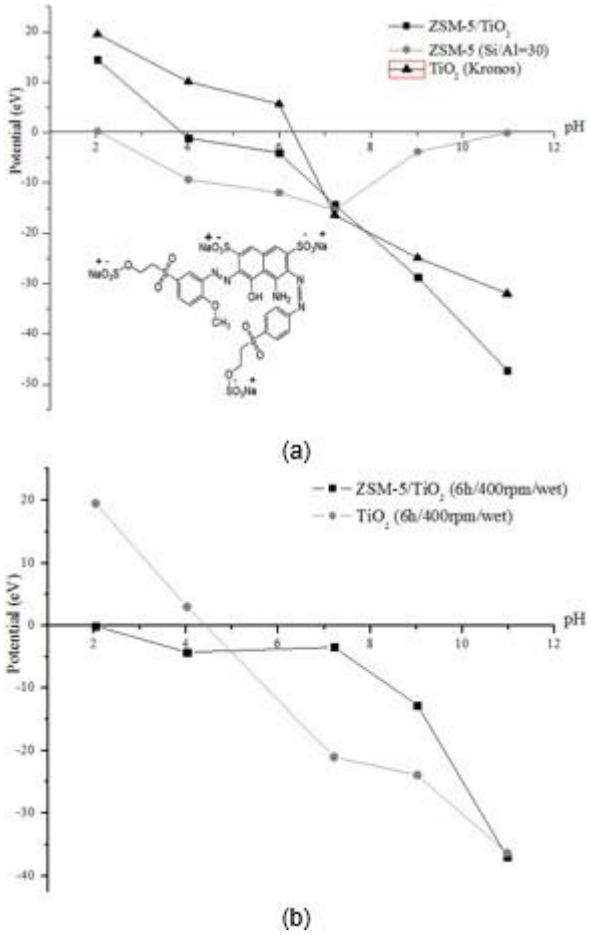

In the photocatalytic tests, the application of non-supported catalysts (Figure 5A) indicated that the best results were from the following catalysts: TiO_2 (6h/400rpm/wet), TiO_2 (without milling) and TiO_2 (10min/300rpm/dry), c.a. 100, 99 and 98% respectively.

Figure 5. Photocatalytic tests for (a) unsupported catalysts, (b) supported TiO2 on ZSM-5(Si/Al=30). %TiO2 = 7%, 6h of reaction with a 250W Hg lamp.

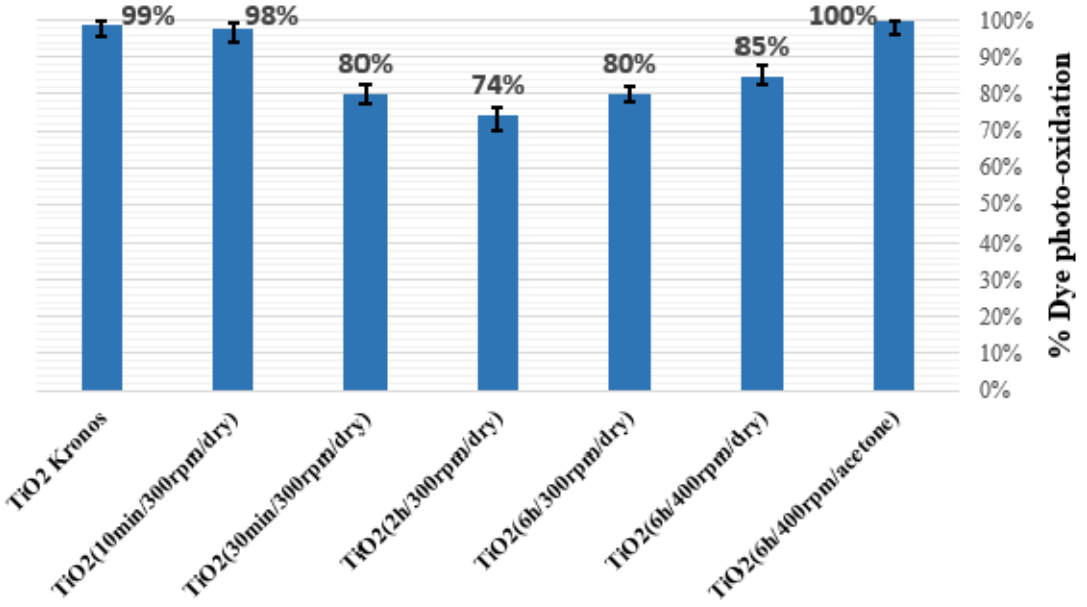

(a)

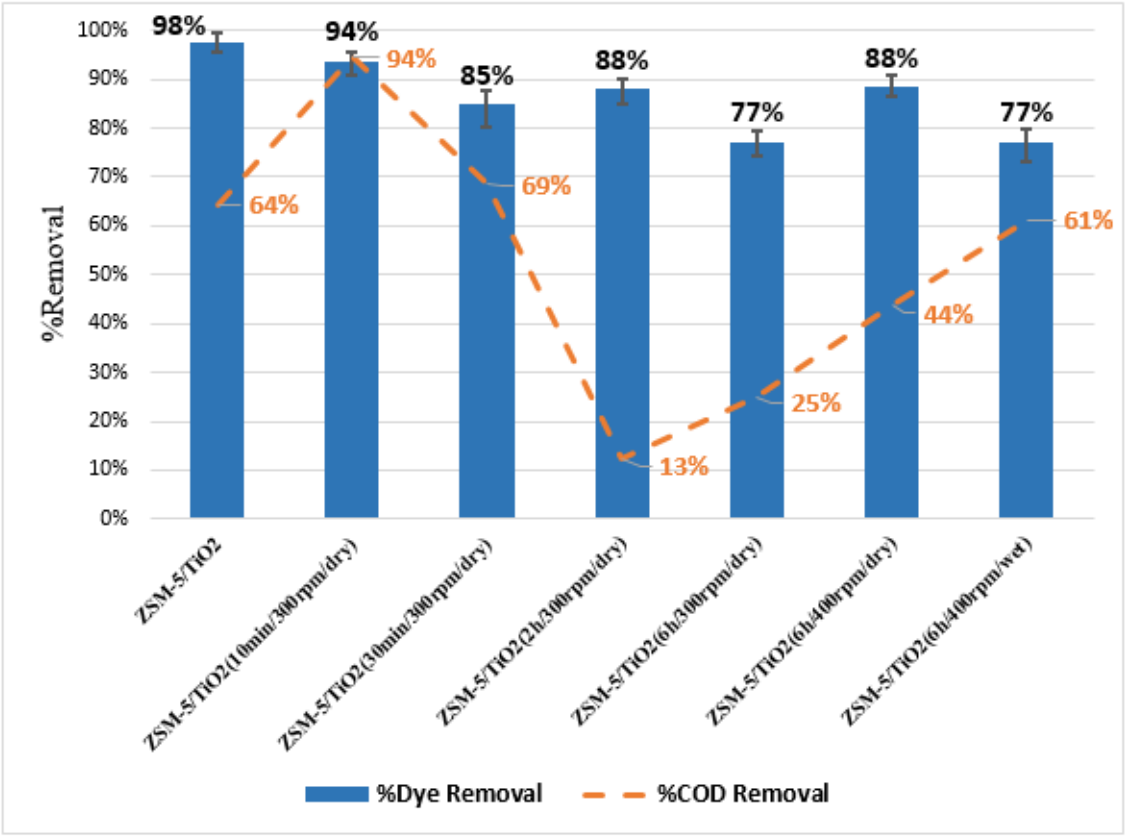

(b)

The catalyst reduces its activity as the concentration of the rutile phase in its composition increases, like reported by Xu *et al* [32] and Jang *et al* [33]. An ideal mix of these two oxides could also imply a good yield of discoloration owing to a formation of

heterojunction within these two phases, increasing the electron transfer (Table 3 and Figure 5A), like indicated by the samples TiO_2 (10 min/ 300 rpm/ dry) and TiO_2 (6 h/ 400 rpm/ wet) [16,33]. According to Fox & Dulay [34] the low activity of the rutile phase ahead of anatase is due to the inability to adsorb O_2 increasing the speed of the electron recombination, which emits radiation in the form of heat and soon causes the catalyst deactivation.

Furthermore, another reasons could be explored concerning to iron contamination to justify the photocatalytic results presented above, caused by the percentual differences along the treated samples (Table 3) [35]. By Mössbauer Technique it was identified the type of iron oxides presents in TiO_2 treated samples, different from XRD analysis, that it was not possibly caused by the lower concentration of iron oxides.

According to the hyperfine parameters obtained by Mössbauer spectroscopy (for wet milled sample) the Fe(III) was present in the form of two sub-spectrums: a doublet distributed and sextet discreet, considering the range of the isomeric shift (δ) for Fe^{3+} of 0.2-0.7 mm/s (Figure 6).

Figure 6. Mössbauer spectroscopy for the TiO2 treated with respective grinding parameters 6h/400rpm/wet.

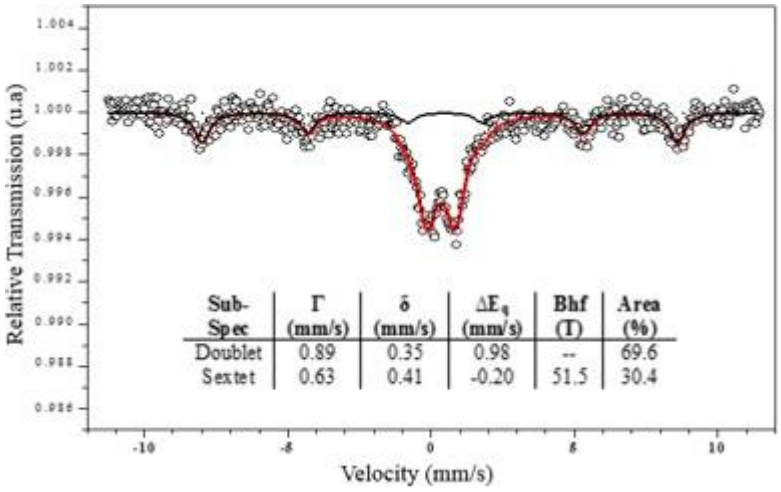

The doublet distributed is related to pseudobrookite (Fe_2TiO_5), which consists in two sites: a greater quadrupole doublet (Deployment quadrupole, ΔE, equal to 0.92 mm/s) together with one doublet with a small area and quadrupole (ΔE = 0.60 mm/s). The lower doublet is located in the form of shoulders on the sidelines of the pseudobrookite spectrum [36]. It may be explained the origin value of 0.98 mm/s for deployment quadrupole, an overlap of the two sites, as discussed by Pal *et al* [37]. Another factor that marks the presence of pseudobrookite is the absence of magnetic field. The sextet discreet indicates hematite (Fe_2O_3), since the magnetic field 51.5 T and ΔE equal to -0.20 mm/s

corroborating the literature [38–40]. The pseudobrookite appears in greater quantity, with 69.6 against 30.4% of hematite, it implies that the pseudobrookite exerts greater influence on the TiO_2 matrix than hematite. In addition, the catalyst activity (Figure 5) could also be reduced with the increase in the percentage of pseudobrookite, causing its corrosion through the high electronic recombination.

Referring to the supported catalysts (Figure 5B) the major photodiscoloration yield was identified to ZSM-5/TiO_2 followed by ZSM-5/TiO_2 (10min/300rpm/dry), 98 and 94%, in order. The reduction identified was in accordance to the reduction in acidity, that implies in minus oxidative agents' generation through water hydrolysis (Table 3). However, the dye photodegradation estimated by COD measurements from ZSM-5/TiO_2 (10min/300rpm/dry) catalyst showed the best results. c.a. 94%, and indicated that this catalyst produced less carbonaceous sub-products than other ones, showing the best mineralization into innocuous compounds CO_2 e H_2O. As a result, the catalyst ZSM-5/ TiO_2 (10min/300rpm/dry) helped to achieve treated and less harmful residual water, with low carbon liquid products contents.

The presence of Fe_2TiO_5 decrease the TiO_2 photocatalytic activity, according to Rodríguez-Torres *et al* [14] and Pal *et al* [37]. Although the band gap energy of pseudobrookite is 2.19 eV and the photocatalytic activity of this iron oxide is very low. This is explained by Pal *et al* [37], by low electron charge transfer to the adsorbed water during the irradiation time, reducing the speed of the redox reactions on the metal surface, causing an accumulation of e^-/h^+ which causes the immediate recombination. Being pseudobrookite the iron oxide form in highest concentration (Figure 6), it causes the reduction on photocatalytic activity (Figure 5).

The kinetics of the reactions as can be observed in Table 5 obeys the first order kinetics due to the greater R-square obtained.

Table 5. Chemical kinetics of the reactions for TiO2 milled.

Catalysts	1st order		2nd order	
	k(s^{-1})	R-square	k(s^{-1})	R-square
TiO_2 Kronos	0.971±0.139	0.97	3.392±2.377	0.17
TiO_2(10min/300rpm/dry)	0.712±0.093	0.99	0.745±0.263	0.58
TiO_2(30min/300rpm/dry)	0.285±0.033	0.98	0.069±0.013	0.83
TiO_2(2h/300rpm/dry)	0.259±0.025	0.97	0.052±0,009	0.85
TiO_2(6h/300rpm/dry)	0.313±0.013	0.99	0.075±0.010	0.93
TiO_2(6h/400rpm/dry)	0.352±0.022	0.98	0.101±0.017	0.87
TiO_2(6h/400rpm/acetone)	1.163±0.112	0.96	6.381±2.091	0.63

The iron oxides contamination could be avoided using grinding balls and a grinding vessel, both constructed with Ti in spite of Fe-Cr-Ni alloy. This care could avoid direct contamination, favoring only the phase change of the TiO_2 and the reduction of the crystallite size, and thus promote the synthesis of more effective catalysts in the degradation of pollutants.

The low percentage of discoloration from ZSM-5/TiO_2 (6h/400rpm/wet) in comparison with the non-supported TiO_2 (6h/400rpm/wet) may cause by synergetic effect with zeolite and titanium oxide, like light scattering caused by the zeolite presence, that blockage part of the photons that should promote the electrons excitations from the active phase of the catalysts.

4 CONCLUSIONS

The TiO_2 samples treated in the mill had 75 % reduction in the particle size. An almost complete transformation of anatase to rutile phase was also observed through energy increase in the process of comminution (microscopic temperature increase). There was also a slight contamination with pseudobrookite and hematite when the grinding system was more energetic with respective parameters of 6h, 400 rpm and dry medium. The best catalyst tested was ZSM-5/TiO_2 (10min/300rpm/dry) achieving 94% discoloration and 94% of COD removal, which indicated the best heterojunction of anatase and rutile phases. These results were justified by a zeolite stronger acidity and greater content of anatase phase. The presence of pseudobrookite and rutile phase in major quantity may also reduce the activity of the catalysts

For future work, the authors recommend the use of a vase and grinding balls of the same composition as the material to be comminuted, in order to avoid contamination with ions that can harm the future application of comminuted powder. They also suggest that more comprehensive statistical planning be done with the grinding parameters in order to account for the effect of each of them isolated and combined in reducing particle size and changing the phase from anatase to rutile.

ACKNOWLEDGEMENTS

The authors gratefully acknowledge the financial support from CNPq and the Complex of Research Support Centers (COMCAP).

REFERENCES

[1] Brites FF, Santana VS, Fernandes-Machado NRC. Effect of support on the photocatalytic degradation of textile effluents using Nb2O5 and ZnO: Photocatalytic degradation of textile dye. Top Catal 2011;54:264–9. https://doi.org/10.1007/s11244-011-9657-2.

[2] Körlü AE, Yapar S, Perinçek S, Yılmaz H, Bağıran C. Dye removal from textile waste water through the adsorption by pumice used in stone washing. Autex Res J 2015;15:158–63. https://doi.org/10.1515/aut-2015-0012.

[3] Vicentini JCM, Medeiros GB, Watanabe MCC, Piccoli KR, Camilo FC, Scaliante MHNO. Synergistic effect between oxides semiconductors and zeolites on photobleaching of RB250 textile dye. Acta Sci - Technol 2018;40:1–8. https://doi.org/10.4025/actascitechnol.v40i1.36553.

[4] Znad H, Abbas K, Hena S, Awual MR. Synthesis a novel multilamellar mesoporous TiO2/ZSM-5 for photo-catalytic degradation of methyl orange dye in aqueous media. J Environ Chem Eng 2018;6:218–27. https://doi.org/10.1016/j.jece.2017.11.077.

[5] Subtil GW, Vicentini JCM, Cordeiro PHY, Scaliante MHNO. Fotodegradação De Corante Textil Azul Rb 250 E Produção Fotocatalítica De H2 Utilizando Tio2 Nano Suportado Em Zeolita Zsm-5 / Rb 250 Blue Dye Photodegradation and H2 Photocatalytic Production Using Tio2 Nano Supported on Zeolite Zsm-5. Brazilian J Dev 2020;6:67238–48. https://doi.org/10.34117/bjdv6n9-236.

[6] Saggioro EM, Oliveira AS, Moreira JC. Heterogeneous Photocatalysis Remediation of Wastewater Polluted by Indigoid Dyes. Text Wastewater Treat 2016. https://doi.org/10.5772/63790.

[7] Goedecke C, Sojref R, Nguyen TY, Piechotta C. Immobilization of photocatalytically active TiO2 nanopowder by high shear granulation. Powder Technol 2017;318:465–70. https://doi.org/10.1016/j.powtec.2017.06.025.

[8] Suryanarayana C. Mechanical alloying and milling. Mech Alloy Milling 2004:1–472. https://doi.org/10.4150/kpmi.2006.13.5.371.

[9] Anand K, Varghese S, Kurian T. Preparation of ultra-fine dispersions of zinc oxide by simple ball-milling: Optimization of process parameters. Powder Technol 2015;271:187–92. https://doi.org/10.1016/j.powtec.2014.11.009.

[10] Jung HJ, Sohn Y, Sung HG, Hyun HS, Shin WG. Physicochemical properties of ball milled boron particles: Dry vs. wet ball milling process. Powder Technol 2015;269:548–53. https://doi.org/10.1016/j.powtec.2014.03.058.

[11] Furlani E, Aneggi E, de Leitenburg C, Maschio S. High energy ball milling of titania and titania-ceria powder mixtures. Powder Technol 2014;254:591–6. https://doi.org/10.1016/j.powtec.2014.01.075.

[12] Dabhade V V., Rama Mohan TR, Ramakrishnan P. Nanocrystalline titanium powders by high energy attrition milling. Powder Technol 2007;171:177–83. https://doi.org/10.1016/j.powtec.2006.10.007.

[13] Miszczak S, Pietrzyk B. Anatase–rutile transformation of TiO2 sol–gel coatings deposited on different substrates. Ceram Int 2015;41:7461–5. https://doi.org/10.1016/j.ceramint.2015.02.066.

[14] Rodríguez-Torres CE, Cabrera AF, Errico LA, Adn C, Requejo FG, Weissmann M, et al. Local structure and magnetic behaviour of Fe-doped TiO2 anatase nanoparticles: Experiments and calculations. J Phys Condens Matter 2008;20. https://doi.org/10.1088/0953-8984/20/13/135210.

[15] Hanaor DAH, Sorrell CC. Review of the anatase to rutile phase transformation. J Mater Sci 2011;46:855–74. https://doi.org/10.1007/s10853-010-5113-0.

[16] Kordouli E, Bourikas K, Lycourghiotis A, Kordulis C. The mechanism of azo-dyes adsorption on the titanium dioxide surface and their photocatalytic degradation over samples with various anatase/rutile ratios. Catal Today 2014.

[17] Petkowicz DI, Pergher SBC, da Silva CDS, da Rocha ZN, dos Santos JHZ. Catalytic photodegradation of dyes by in situ zeolite-supported titania. Chem Eng J 2010;158:505–12. https://doi.org/10.1016/j.cej.2010.01.039.

[18] Opalka SM, Zhu T. Influence of the Si/Al ratio and Al distribution on the H-ZSM-**5** lattice and Brønsted acid site characteristics. Microporous Mesoporous Mater 2016;222:256–70. https://doi.org/10.1016/j.micromeso.2015.10.030.

[19] Jenkins R, Snyder R. Introduction to X-Ray Powder Diffractometry. Wiley & Sons Ltd; 1996.

[20] Chen W, Liu M, Wang Y, Gao L, Dang H, Mao L. Non-noble metal Co as active sites on TiO 2 nanorod for promoting photocatalytic H 2 production. Mater Res Bull 2019;116:16–21. https://doi.org/10.1016/j.materresbull.2019.04.011.

[21] Nguyen NT, Ozkan S, Hejazi S, Denisov N, Tomanec O, Zboril R, et al. Providing significantly enhanced photocatalytic H2 generation using porous PtPdAg alloy nanoparticles on spaced TiO2 nanotubes. Int J Hydrogen Energy 2019;44:22962–71. https://doi.org/10.1016/j.ijhydene.2019.06.200.

[22] Deshmane VG, Owen SL, Abrokwah RY, Kuila D. Mesoporous nanocrystalline TiO<inf>2</inf> supported metal (Cu, Co, Ni, Pd, Zn, and Sn) catalysts: Effect of metal-support interactions on steam reforming of methanol. J Mol Catal A Chem 2015;408:202–13. https://doi.org/10.1016/j.molcata.2015.07.023.

[23] Ghosh P, Chelli VR, Giri AS, Golder AK. Steroid glycosides as potential analytes for Cu-doping on TiO 2 for photocatalytic water treatment. Environ Prog Sustain Energy 2018;37:1973–81. https://doi.org/10.1002/ep.12879.

[24] Arul AR, Manjulavalli TE, Venckatesh R. Visible light proven Si doped TiO2 nanocatalyst for the photodegradation of Organic dye. Mater Today Proc 2019;18:1760–9. https://doi.org/10.1016/j.matpr.2019.05.275.

[25] Ali MHH, Al-Afify AD, Goher ME. Preparation and characterization of graphene – TiO2 nanocomposite for enhanced photodegradation of Rhodamine-B dye. Egypt J Aquat Res 2018;44:263–70. https://doi.org/10.1016/j.ejar.2018.11.009.

[26] Tauc J, Grigorovici R, Vancu A. Optical Properties and Electronic Structure of Amorphous Germanium. Phys Status Solidi 1966;15:627–37. https://doi.org/10.1002/pssb.19660150224.

[27] Arzenšek D, Podgornik R, Kuzman D. Dynamic light scattering and application to proteins in solutions. Seminar 2010:1–18.

[28] Nejat T, Jalalinezhad P, Hormozi F, Bahrami Z. Hydrogen production from steam reforming of ethanol over Ni-Co bimetallic catalysts and MCM-41 as support. J Taiwan Inst Chem Eng 2019;97:216–26. https://doi.org/10.1016/j.jtice.2019.01.025.

[29] Brites-Nóbrega FF, Lacerda IA, Santos S V., Amorim CC, Santana VS, Fernandes-Machado NRC, et al. Synthesis and characterization of new NaX zeolite-supported Nb, Zn, and Fe photocatalysts activated by visible radiation for application in wastewater treatment. Environ Sci Technol 1995;29:240.

[30] Kosmulski M. pH-dependent surface charging and points of zero charge. IV. Update and new approach. J Colloid Interface Sci 2009;337:439–48. https://doi.org/10.1016/j.jcis.2009.04.072.

[31] Kosmulski M. The pH-dependent surface charging and points of zero charge. V. Update. J Colloid Interface Sci 2011;353:1–15. https://doi.org/10.1016/j.jcis.2010.08.023.

[32] Xu N, Shi Z, Fan Y, Dong J, Shi J, Hu MZC. Effects of particle size of TiO2 on photocatalytic degradation of methylene blue in aqueous suspensions. Ind Eng Chem Res 1999;38:373–9. https://doi.org/10.1021/ie980378u.

[33] Jang HD, Kim SK, Kim SJ. Effect of particle size and phase composition of titanium dioxide nanoparticles on the photocatalytic properties. J Nanoparticle Res 2001;3:141–7. https://doi.org/10.1023/A:1017948330363.

[34] Fox MA, Dulay MT. Heterogeneous Photocatalysis. Chem Rev 1992:135–70. https://doi.org/10.1016/B978-0-444-53178-0.00004-3.

[35] Li X, Zhu K, Pang J, Tian M, Liu J, Rykov AI, et al. Unique role of MÖssbauer spectroscopy in assessing structural features of heterogeneous catalysts. Appl Catal B Environ 2018;224:518–32. https://doi.org/10.1016/j.apcatb.2017.11.004.

[36] Rodríguez-Torres CE, Cabrera AF, Van Raap MBF, Sánchez FH. Mössbauer study of mechanical alloyed Fe-doped TiO2 compounds. Phys B Condens Matter 2004;354:67–70. https://doi.org/10.1016/j.physb.2004.09.023.

[37] Pal B, Sharon M, Nogami G. Preparation and characterization of TiO2/Fe2O3 binary mixed oxides and its photocatalytic properties. Mater Chem Phys 1999;59:254–61. https://doi.org/10.1016/S0254-0584(99)00071-1.

[38] Lemine OM, Sajieddine M, Bououdina M, Msalam R, Mufti S, Alyamani A. Rietveld analysis and Mössbauer spectroscopy studies of nanocrystalline hematite α-Fe2O3. J Alloys Compd 2010;502:279–82. https://doi.org/10.1016/j.jallcom.2010.04.175.

[39] Kalska-Szostko B, Satuła D, Olszewski W. Mössbauer spectroscopy studies of the magnetic properties of ferrite nanoparticles. Curr Appl Phys 2015;15:226–31. https://doi.org/10.1016/j.cap.2014.12.011.

[40] Cristóbal AA, Ramos CP, Botta P, Aglietti EF, Saragovi C, Porto JM. Characterization of a mechanochemically activated titanium-hematite mixture: Mössbauer spectroscopy study. Phys B Condens Matter 2009;404:2751–3. https://doi.org/10.1016/j.physb.2009.06.075.